BIOCHEMISTRY
including biophysical chemistry & molecular biology

ARTICLE

pubs.acs.org/biochemistry

Contributions of Glycosaminoglycan Binding and Clustering to the Biological Uptake of the Nonamphipathic Cell-Penetrating Peptide WR_9

André Ziegler* and Joachim Seelig

Department of Biophysical Chemistry, Biozentrum, University of Basel, Klingelbergstrasse 50/70, 4056 Basel, Switzerland

ABSTRACT: Many cell-penetrating peptides (CPPs) bind to glycosaminoglycans (GAG) located on the extracellular side of biological tissues. CPP binding to the cell surface is intimately associated with clustering of surface molecules and is usually followed by uptake into the cell interior. We have investigated the uptake mechanism by comparing CPPs which bind, but cannot induce, GAG clustering with those which do induce GAG clustering. We have synthesized the tryptophan-labeled CPP nona-L-arginine (WR_9) and its monodispersely PEGylated derivate (PEG_{27}—WR_9) and have compared them with respect to glycan binding, glycan clustering, and their uptake into living cells. Both CPPs bind to the GAG heparin with high affinity ($K_D \sim 100$ nM), but the PEGylation prevents the GAG clustering. Thus, it is possible to uncouple and analyze the contributions of GAG binding and GAG clustering to the biological CPP uptake. The uptake of PEG—WR_9 into CH-K1 cells is confined to intracellular vesicles, where colocalization with transferrin attests to an endocytic uptake. Transfection experiments with plasmid DNA for GFP revealed poor GFP expression, suggesting that endocytic uptake of PEG—WR_9 is compromised by insufficient release from endocytic vesicles. In contrast, WR_9 shows two uptake routes. At low concentration (<5 μM), WR_9 uptake occurs mainly through endocytosis. At higher concentration, WR_9 uptake is greatly enhanced, showing a diffuse spreading over the entire cytoplasm and nucleus—a phenomenon termed "transduction". Transduction of WR_9 leads to a higher GFP expression as compared to PEG—WR_9 endocytosis but also damages the plasma membrane as evidenced by SYTOX Green staining. The results suggest that GAG binding without and with GAG clustering induce two different pathways of CPP uptake.

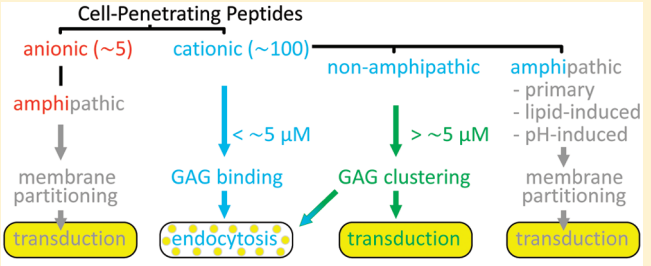

Approximately 60% of currently FDA-approved drugs bind to membrane proteins as their molecular target[1] inducing their biological activity either directly (e.g., anesthetics) or indirectly via signaling across the cell membrane (e.g., receptor blocker). Future drug technologies will address intracellular targets which emerge from recent discoveries in genomics, proteomics, and glycomics. These molecular pathways can be temporarily manipulated at several levels, such as gene expression with plasmids, siRNA, and intracellular antibodies.[2] The applicability of these technologies will depend critically on transporting the rather large therapeutic molecules across intact cell membranes, a major hurdle for their clinical use.

While the lipid bilayer is impermeable to large macromolecules, such as tailored DNA/RNA strands, because of their size (Lipinski's rule)[3] and high charge (Born energy barrier),[4] their cellular uptake can be enhanced by uptake promoting compounds ("vectors") such as viral peptides, lipofectants, synthetic polymers (polybrene, polyethylenimine), amino acid homopolymers,[5] and cell-penetrating peptides (CPPs).[6,7]

Among these vectors, CPPs are of particular interest because of their rapid uptake into the cytoplasm and the cell nucleus, their biodegradability, and the responsiveness of many diverse cell lines to CPPs. For example, the uptake of CPPs has been observed not only in various mammalian cell lines but also in bacterial, yeast, insect, and plant cells that differ considerably in their membrane composition and, especially, in their capacity for endocytosis.[8] The CPP uptake into biological cells proceeds typically within minutes at a low micromolar CPP concentration. The potential cargos can be bound either covalently or electrostatically to the CPP. Apart from numerous CPPs studied on cells in culture and occasionally in rodents, first clinical trials on humans are currently in progress for drugs like AVI-5126,[9,10] ANG1005,[11] KAI-9803,[12] Syn1001,[13] and CGC1072[14] that are based on CPPs.

With a few exceptions, most CPPs have a high content of arginine and lysine residues, so that their isoelectric point (pI) is typically >10, which leads to a net positive charge at physiological pH and facilitates electrostatic interactions with anionic cargos (e.g., DNA) and cellular targets (e.g., cell-surface glycans). Polycationic characteristics are also found for other, non-peptide transfection vectors such as Lipofectamine, polyethylenimine, polybrene, chitosan, or DEAE-dextran. It is believed that their polycationic property facilitates the cellular uptake of elongated anionic cargos, such as plasmid DNA, by at least six additive

Received: December 6, 2010
Revised: April 12, 2011
Published: April 14, 2011

processes: noncovalent binding to the cargo, compaction of the large cargo, resulting protection against enzymatic digestion (e.g., ubiquitous RNases), charge (over)neutralization (defeating the Born energy barrier), sedimentation of the compact aggregates onto cell layers, and increase of the cell surface concentration through residual positive charges by electrostatic interaction with anionic cell-surface molecules like sulfated or sialylated glycans.

The residual positive charge of the vector−cargo complex appears to be mandatory for optimum plasmid expression, where a charge ratio (cationic N/anionic P) of 2−5 typically yields best transfection efficiency[15] by providing contact to anionic cell-surface molecules. The involvement of anionic cell-surface glycans in the CPP uptake is also supported by enzymatic removal of diverse glycans from the cell surface[16−18] and the observation that D-isomers and retro-inverso derivatives of CPPs enter cells with a similar efficiency as their L-isomers.[19] In contrast, a purely protein-based receptor would be stereospecific due to its natural L-isomer composition.

The biological cell response after the initial cell-surface contact of CPPs is discussed controversially, not only because of large structural differences among CPPs but also because of different experimental conditions, different cell lines used (differing in endocytic capacity), different cargo sizes,[20] and potential artifacts during cell handling. For example, the high cell-surface accumulation of CPPs has occasionally been mistaken as intracellular uptake when using FACS.[21] Also, the cell fixation with aldehydes or methanol used in microscopy leads to leaky cell membranes, so that the cell surface-bound CPP diffuse "artificially" into the cytosol postmortem.[22] Such artifacts accidentally suggested that the uptake of nonamphipathic CPPs was independent of cellular energy consumption.[23] This early view was corrected later, and in order to clarify, it was necessary (i) to divide the CPPs at least into two classes, i.e., amphipathic and nonamphipathic CPPs,[8,24] and (ii) to consider various uptake pathways for one and the same CPP as a function of concentration or other conditions. As a result of their physicochemical properties, CPPs might indeed produce membrane leakage in the absence of cellular fuels. The classes of CPPs are thus distinct with respect to leakage on model membranes, toxicity on cells in culture, and cellular uptake routes (for a review see ref 8).

Amphipathic CPPs, such as transportan and pep-1, have detergent-like properties.[25] They insert into the lipid bilayer core, and the threshold for causing energy-independent membrane leakage has been found to be as low as 1 μM.[26] Importantly, the membrane partitioning and leakage of amphipathic CPPs can be produced in model membrane systems devoid of glycans or related core proteins.[25] Their membrane destabilization is thus in close similarity to antimicrobic peptides.[27] Their partitioning into the lipid bilayer and resulting membrane leakage does not exclude the possibility for a parallel endocytic uptake, and it seems that the CPP concentration affects both the uptake route and the toxicity.[8] Their *diffuse* intracellular distribution has been referred as to "transduction", i.e., peptide passage across a membrane.[28] At that time, the designation "transduction" was not restricted to "cytosolic" appearance in particular but to intracellular appearance in general *including* entrapment in endocytic vesicles. Entrapment of fluorescently labeled CPPs in the endosome typically produces a punctuate intracellular staining of the cells especially in the time frame of our experiments. We use the term "transduction" in the present article thus for the *diffuse* cytosolic CPP localization, indicating that the CPP has crossed a cellular membrane without specifying the location of the membrane leak (see also Discussion).

In contrast, nonamphipathic CPPs, such as oligoarginines, are polyelectrolytes that have no detergent-like or pore-forming property. They have a poor affinity for lipids that are typical for the outer membrane leaflet of the eukaryotic plasma membrane; they do not insert into model lipid bilayers and do not produce membrane leakage of lipid vesicles at low micromolar concentration.[8] Their membrane leakage on model membranes has been only observed at very special conditions, such as lipid-phase transition cycling, unnatural counterions, high molar peptide/lipid ratios, or membrane models with low bending modulus (GUVs).[8] Formation of inverted hexagonal phases has been also proposed as a lipid-mediated uptake mechanism but has not been experimentally confirmed so far.[25]

Nevertheless, nonamphipathic CPPs have substantial access to cytosol and nucleus.[29−32] This suggests that cell-membrane constituents other than lipids are responsible for the transduction of nonamphipathic CPPs. We have shown previously that glycosaminoglycans (GAGs) may play an important role in this process.[29] The present article thus focuses on the special properties of nonamphipathic CPPs. Among those, we have selected nona-L-arginine (WR_9), which is considered as one of the most effective CPPs among the arginine homologues.[33]

We have first investigated the conditions for endocytic uptake and transduction of the nonamphipathic CPP WR_9. Second, we have tested to which extend glycan clustering may contribute to the WR_9 uptake because a previous study suggested that the transduction of nonamphipathic CPPs is closely related to the cell-surface clustering of CPPs.[34] Third, a PEGylated CPP variant was synthesized that, in contrast to typical CPPs, should bind with high affinity to GAGs but should inhibit glycan clustering. After biophysical characterization of the interactions, we have measured the CPP uptake into CHO-K1 cells in culture, the toxicity, and the transfection efficiency for a GFP plasmid.

EXPERIMENTAL PROCEDURES

Materials. Fmoc-protected amino acids were purchased from Iris Biotech (Marktredwitz, Germany). The peptide activators HBTU and PyBop were obtained from VWR (Dietikon, Switzerland), and the resins for peptide synthesis were purchased from Rapp Polymere (Tübingen, Germany). The monodisperse, bifunctional PEG reagent 3-(2-(2-(9-Fmoc)aminoethoxy)-$(ethoxy)_{27}$)propanoic acid ("Fmoc-NH-PEG_{27}-COOH"; M_r = 1544.8) was purchased from Polypure (Norway, Oslo). The fluorescent 5(and 6)-carboxytetramethylrhodamine (TAMRA) succinimidyl ester (SE) was from Anawa/Anaspec (Wangen, Switzerland). Unfractionated heparin sodium salt (from porcine intestinal mucosa, 12.4% sulfur, average $M_r \sim 13\,000$) was purchased from Celsus Laboratories (Cincinnati, OH). The reporter plasmid gWiz-GFP (5757 base pairs) was obtained from Aldevron (Fargo, ND). SYTOX Green, Lipofectamine 2000, cell culture media (Opti-MEM; F-12 with GlutaMAX), and supplements (serum, antibiotics) were from LuBioScience/Invitrogen (Luzern, Switzerland). CellTiter 96 aq was from Promega (Dübendorf, Switzerland). DyLight 488-labeled rat transferrin was from Jackson Immuno (Suffolk, GB). All other chemicals (synthesis or HPLC grade) were purchased from Sigma-Aldrich (Buchs, Switzerland). The DNA concentration (as base pair) was determined spectroscopically using an average

molar extinction coefficients per base pair (ε_{260} = 13 200 M^{-1} cm^{-1}).[35]

Peptide Synthesis. Solid phase peptide synthesis (0.1 mmol scale = 1 mol equiv) started on the peptide's C-terminus using a Tentagel S RAM Rink-type resin (functionalization of 0.24 mmol/g) and *N*-(9-fluorenyl)methyloxycarbonyl (Fmoc) protected amino acids (10 equiv) on an Applied Biosystems 433A peptide synthesizer (Stafford, TX). Activation reagents were HBTU/HOBt/DIPEA (10:10:20 equiv). A more porous resin (Tentagel R RAM; functionalization of 0.18 mmol/g) was required for the synthesis of the PEGylated derivative in order to facilitate the rapid diffusion of the larger PEG moiety into the resin with respect to the short half-life of the activated reagents after addition of DIPEA.

Fmoc-NH-PEG(27)-COOH was coupled by hand (3 equiv, 4 h) at the N-terminus using activation with PyBOP/DIPEA (3:6 equiv) in DMF/DCM (9:1). The bifunctional PEG spacer allowed fluorescent labeling of the peptide after Fmoc deprotection with 20% piperidine. The resin and side-chain protection groups were removed with Reagent B (TFA/phenol/H_2O/triisopropylsilane 88:5:5:2) while stirring under argon in the dark (2 h). The crude peptides were precipitated in ice-cooled *tert*-butyl methyl ether and lyophilized. They were purified on a preparative HPLC (Gilson 321, Villiers le Bel, France) using a C_8 column (Lichrosorb RP-8/250-25, Merck, Darmstadt, Germany) at a flow rate of 15 mL/min and a linear elution gradient from 5 to 55% acetonitrile (0.1% TFA) within 50 min. At these conditions, H_2N-WRRRRRRRRR-$CONH_2$ ("WR_9") and H_2N-PEG(27)-WR_9-$CONH_2$ ("PEG−WR_9") eluted at 24.2 and 36.7 min, respectively. Peptide purity (>95%) was measured by analytical HPLC using a HP1050 (Agilent Technologies, Waldbronn, Germany). The mass of the peptides was measured by MALDI-TOF mass spectrometry using a DHB matrix and a Voyager-DE Pro spectrometer (Applied Biosystems; Foster City, CA) operating in positive reflector mode. Because of the Rink amide linker at the resin, the peptides were released as an amidated (uncharged) C-terminus after cleavage with TFA. After purification, the peptides were suspended in water, neutralized to pH 7.40, and lyophilized twice from water. The peptide concentration in solutions was determined spectroscopically using the molar extinction coefficients of tryptophan (ε_{280} = 5500 M^{-1} cm^{-1}).[36]

Fluorescent Markers. The resin-bound and side-chain protected peptides (0.02 mmol, 1.0 equiv) were fluorescently labeled at the N-terminus using a mixture of 5(6)-TAMRA SE (3.0 equiv) and DIPEA (6.0 equiv) in 2 mL of anhydrous DMF. TAMRA was preferred over FITC because of its stable fluorescence at low endosome pH, little photobleaching, and also wavelength compatibility with the other stains used (e.g., SYTOX Green). Cleavage from the resin and purification were done in analogy to the nonfluorescent peptides.

Isothermal Titration Calorimetry (ITC). The binding of the peptides to GAGs or plasmid DNA was measured on a iTC_{200} (GE Healthcare/Microcal; Northampton, MA) and a TAM-III 2277 (ThermoMetric AB; Järfälla, Sweden) calorimeter using a multisite binding model for the analysis.[34] Dissociation constants K_D are calculated as $1/K$.

Dynamic Light Scattering (DLS). The reactant solutions were filtered (PES; 0.22 μm; Millipore; Billerica, MA) prior to mixing. DLS and zeta potential measurements were performed on a Zetasizer Nano ZS ZEN3600 (Malvern; Worcestershire, UK) equipped with a HeNe laser (633 nm) and a backscattering detection (scattering angle of 173°). Measurements were performed in 1 cm rectangular cuvettes at 25 °C. The intensity autocorrelation functions were evaluated using a second-order cumulant analysis yielding the translational diffusion coefficient D. The mean hydrodynamic diameter (D_H) was calculated from D by using the Stokes−Einstein equation. The size distributions were calculated from the diffusion coefficient distribution using the CONTIN routine, and the resulting intensity counts were volume-weighted.

Analytical Ultracentrifugation (AUC). AUC data were measured on a Beckman XL-I (Beckman Coulter, Indianapolis, IN) equipped with UV- and interference detection.

Cell Culture. Wild-type Chinese hamster ovary cells, CHO-K1 (ATCC; Manassas, VA), were grown in Ham's F12 medium (containing GlutaMAX instead of glutamine) supplemented with 10% (v/v) fetal bovine serum, 100 U/mL penicillin, and 100 μg/mL streptomycin using 75 cm^2 large vented cell culture flasks (BD Biosciences; Allschwil, Switzerland). The cells were incubated at 37 °C in humidified air containing CO_2 (5%). Every second day (at ∼80% confluency), the cells were detached (trypsin and EDTA.Na_4 at 0.5 and 0.2 g/L, respectively) and split at a ratio of 1:10 up to a maximum of 25 passages.

Confocal Laser Scanning Microscopy. CHO cells were seeded in 24-well dishes onto sterile noncoated microscopic coverslips (14 mm diameter; Karl Hecht; Sondheim, Germany) and incubated for 48 h in order to obtain a confluency of ∼80%. Thereafter, cells were rinsed with PBS to remove residual FCS and to avoid CPP scavenging by albumin. Subsequently, 0.5 mL of the CPP solution in F-12 medium (containing antibiotics, but no FCS) was added. After 1 h of contact time in the cell incubator, cells were rinsed three times with PBS, mounted upside down on top in 30 μL of Fluoromount G, and imaged immediately for no longer than 15 min. Confocal images were acquired using a Leica TCS-NT-SP1 and SP5 scanning system (Leica Microsystems) using a HC PL APO 20×/NA0.7, HCX PL APO 40×/NA0.85, and adjustable aperture oil-immersion PL APO 100×/NA1.4−0.7 objective. The detection pinhole diameter was set to 1 Airy unit. A diode pumped solid-state yellow laser (561 nm) was used for excitation of TAMRA-labeled CPPs, whereas an argon laser (488 nm) was used for excitation of SYTOX Green, GFP, and DyLight 488-labeled transferrin. In order to detect endocytosis, cells were incubated for 30 min with DyLight 488-labeled transferrin (2 μM in Opti-MEM; containing antibiotics, but no FCS), followed by three times rinsing with PBS and subsequent CPP incubation as described above. Merging of CPP images (red channel) and transferrin images (green channel) was effectuated with the software ImageJ (NIH, Bethesda, MD).

Quantification of CPP Uptake and Protein Content. Proper quantification of CPP uptake requires the removal of superficially bound CPPs by rinsing with buffer, trypsin, and heparin. Especially during WR_9 transduction at high concentrations (>5 μM), some cells were no longer tightly attached to the support, so that extensive heparin rising steps would have caused up to 20% of detached cells (and thus cell loss) in 96-well plates—in contrast to cells showing endocytosis only or to microscopic recordings where the extensive rinsing steps were not used. In order to account for the entire cell population (i.e., transduction and endocytosis), the quantification of intracellular CPPs was performed on larger batches, where cell loss was minimized by recovering detached cells through mild centrifugation of the wash solutions.

In brief, cells were cultured in six-well culture flasks to a confluency of ∼80%. Then, cells were rinsed once with PBS to remove residual FCS. Thereafter, 0.5 mL of the CPP solution in

F-12 medium (containing antibiotics, but no FCS) was added. After a 1 h contact time (cell incubator), cells were rinsed twice with PBS (while still being adherent). This procedure removes unbound CPPs that would interfere with Accutase in the following steps. Some detached cells that might be present after high concentrated WR_9 solutions were recovered from the wash medium by centrifugation (250*g*) and were added again to the adherent cells. Thereafter, cells were rinsed twice with heparin (78 μg/mL). Again, detached cells were recovered by centrifugation. Thereafter, cells were enzymatically detached with Accutase in order to obtain well-dispersed, isolated cells. Especially for FACS measurements, detachment with Accutase (1 mL, 20 min at 37 °C) was preferred over trypsin because WR_9 at high concentrations (>10 μM) leads to partially damaged and agglutinated cells when using trypsin. Finally, cells were rinsed once again with PBS. Subsequently, quantification of the CPP uptake in the entire cell population or in individual cells was performed using cell lysis or FACS, respectively.

In order to quantify the CPP uptake in the cell collective ($\sim 2 \times 10^6$ cells/well), the Accutase-treated cells were lysed for 20 min using 200 μL of lysis buffer (0.1% Triton X-100, 100 mM potassium phosphate, pH 7.8) followed by two freeze/thaw cycles (−80 °C) to ensure complete lysis. Thereafter, 0.4 mL of water was added up, and the fluorescence was quantified using a standard curve of 0.05−2 μM of the fluorescent CPPs in the buffer. As a reference for the cell count, the total cellular protein content was measured by a Bradford protein assay using the protein-binding dye Coomassie brilliant blue G-250 (Serva; Heidelberg, Germany) and a standard curve of 1−10 μg bovine plasma gamma globulin (Bio-Rad; Richmond, VA) per 96-well (250 μL). For this purpose, 20 μL of the cell lysate was mixed with 230 μL of Bradford's solution, and the absorbance was read at 590 nm after 15 min. Occasionally, cell lysate volumes <20 μL were used and completed with lysis buffer to 20 μL, whenever the absorbance was higher than that of the standard curve. Fluorescence and absorbance readings were done with the plate reader SPECTRA max M2 (Molecular Devices; Sunnyvale, CA).

In order to quantify the CPP uptake of individual cells and their viability by FACS, cells were subjected to 1 mL/well of 10 μM of SYTOX Green (10 min) after CPP/PBS exposure and before heparin/Accutase treatment. After the above-described heparin/Accutase/PBS treatments, cells were suspended in 1 mL of PBS and analyzed by FACS using a FACSCantoII (Becton Dickinson, BD Biosciences) counting 10 000 cells/well. Eventual fluorescence spillover of the two fluorochromes was compensated using untreated, SYTOX only, and TAMRA only treated cells. Data were evaluated with the Cyflogic software (CyFlo; Turku, Finland).

Toxicity. Using microscopy (~100 cells/field of view), live and damaged cells after CPP exposure were distinguished using 10 μM of SYTOX Green (ex/em 504/523 nm) in PBS (10 min incubation at 37 °C) followed by the above-mentioned washing and mounting steps. In brief, SYTOX Green penetrates damaged plasma and nuclear membranes producing green fluorescent staining of nucleic acids, whereas cells having an intact plasma membrane are not penetrated and stained by SYTOX Green. When compared to propidium iodide, the emission wavelength of SYTOX Green is distant from TAMRA's emission wavelength, and its fluorescence enhancement is also much higher when bound to nucleic acids. This results in a high sensitivity for detection of damaged cells.

Using spectrophotometry, the active proliferation of $\sim 10^5$ cells/well was quantified in 96-well plates using the CellTiter 96 aq assay after CPP exposure. In contrast to the conventional CellTiter 96 assay, the "aq" type leads to a formazan product that is soluble in tissue culture medium, so that cell extraction is not necessary. In brief, metabolically active cells reduce the tetrazolium salt into a formazan product being soluble in tissue culture medium and detectable at 490 nm, i.e., again distant from TAMRA's aborbance (in contrast to MTT). Monitoring cellular metabolic activity instead of cell membrane exclusion has the advantage of being sensitive to potentially detached cells. In brief, cells were cultured in 96-well plates to ~80% confluency, rinsed once with PBS, and subjected to 0.2−100 μM of CPPs in F-12 medium (containing antibiotics, but no FCS). After a 1 h contact time (cell incubator), cells were rinsed twice with PBS (while still being adherent) and incubated with 100 μL of regular F-12 medium (1 h). Then, 20 μL/well of the CellTiter 96 aq reagent was added, and after a 1 h incubation (37 °C), the formazan production was measured (490 nm) and compared to control cells that were exposed to F-12 instead of the CPPs. An identical incubation time of 1 h was chosen in order to compare the potential membrane leakage (see SYTOX Green assay) with acute effects on cellular viability.

GFP Transfection. The transport efficiency of the CPPs for delivery of a plasmid encoding enhanced green fluorescent protein (gWIZ GFP) was tested and then compared with the commercial lipofectant Lipofectamine 2000. For this purpose, cells were cultured in 96-well plates to ~90% confluency which, according to proprietary information on Lipofectamine, results in least toxicity. Subsequently, cells were rinsed once with PBS and incubated for 1 h with preformed CPP (10 μM)/pDNA complexes in Opti-MEM using 0.2 μg of the plasmid per well. The charge ratio of the peptide's cationic amines (N) to anionic phosphates (P) of the DNA was 2 (N/P), which has been reported to be optimum for transfection.[15] Although the charge ratio for optimum transfection might differ between the CPPs, we have chosen the same charge ratio for both CPPs because of the similar zeta potential of the resulting polyplexes (see Results). FCS was omitted in the transfection medium because of the known interaction of CPPs and lipofectants with serum components.[33] Thereafter, cells were rinsed once with PBS and incubated for 24 h in regular F-12 medium to allow for expression of the GFP. Photographs were taken from the plastic dishes using an inverted fluorescence microscope Nikon Diaphot TMD. The total GFP expression per well was assessed immediately after cell lysis (10 min lysis, no protease inhibitors), where the fluorescence (475/510 nm) and protein content were read as described above.

As a comparison of the CPPs to commercial transfection reagents, Lipofectamine 2000 was used according to the manufacturer's suggestions, i.e. also on 90% confluent cells, applying 0.5 μL of Lipofectamine and 0.2 μg of DNA per 100 μL of OptimMEM. This procedure yields a final concentration of the pentavalent cationic lipid DOSPA of 3.5 μM and a N/P ratio of 2.9 which is similar to the CPP protocol. An equal incubation time of 1 h was used for all 3 reagents. It has been reported that a 4-fold longer incubation time could double the gene expression of Lipofectamine.[37]

RESULTS

High Affinity of WR_9 and PEG−WR_9 for Glycosaminoglycans. We have synthesized the nonamphipathic, tryptophan-labeled

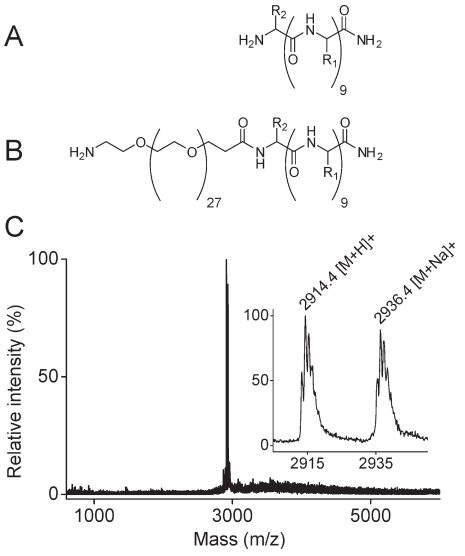

Figure 1. Chemical structure of the peptides used. (A) WR_9 (theoretical M_r = 1608.9) and (B) PEG−WR_9 (theoretical M_r = 2913.5), where R_1 = side chain of arginine and R_2 = side chain of tryptophane. (C) Experimental MALDI-TOF-MS of PEG−WR_9. The insert shows the magnified m/z axis from 2900 to 2950 where proton and sodium adduct ions of PEG−WR_9 are identified.

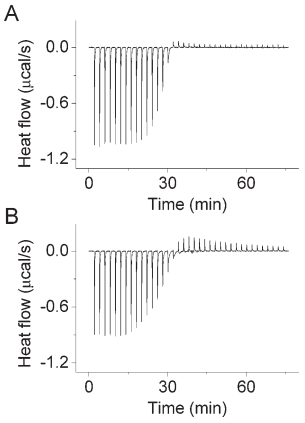

Figure 2. ITC of the GAG−CPP interaction. The reaction cell contains 204 μL of the CPP solution (60 μM), and it is titrated every 2 min with 1 μL of heparin (100 μM, $M_r \sim$ 13 000). Considering formal charge of the molecules, charge neutralization is expected at the 15th injection (Table 1). (A) Titration of WR_9. (B) Titration of PEG−WR_9. Temperature is 37 °C, and buffer is 20 mM Tris, 100 mM NaCl, pH 7.4.

WR_9 and its N-terminus PEGylated derivative PEG−WR_9 whose structures are shown in Figure 1. PEG−WR_9 carries 27 ethylene oxide repeats the brushlike structure of which is expected to prevent aggregation after GAG binding. Binding and clustering of GAGs were found to be coupled for many CPPs.[34] The resulting monodisperse PEG−WR_9 has the same net charge as WR_9 (Figure 1), but a higher relative molecular mass (M_r = 2914). The PEGylation with the monodisperse PEG chain was preferred over a heterodisperse PEG variant obtained via direct linking or resin cleavage because a well-defined mass improves chemical purification and data analysis. After purification, polyelectrolytes, such as WR_9, have counterions, and they are hygroscopic, so that quantification by weight is often biased.[25] Therefore, one tryptophan residue per peptide chain was included in the amino acid sequence (Figure 1) in order to facilitate the peptide quantification by spectroscopic means.

It was first tested whether the PEGylation influences the GAG binding of the 2 CPPs because it is known that PEGylation may prevent not only interparticle aggregation, but also binding of ligands, whenever the PEG chain length or grafting density exceeds a certain threshold.[38]

Using isothermal titration calorimetry (ITC), a micromolar solution of the CPP was titrated every 2 min with the GAG solution. The repeated GAG injections produced a heat release until all CPP was bound to the GAG macromolecule. This occurred approximately at injection number 15, as shown in Figure 2. Thereafter, the GAG injections did not produce any significant heat change. Integration of the heat flow produced the heat of binding for each injection which could be translated into a binding isotherm which was further analyzed using a multisite binding model.[34] In brief, the large anionic GAG polyelectrolyte was assumed to have n identical binding sites with the microscopic dissociation constant (K_D) for the much smaller CPP. Figure 2 demonstrates that both CPPs bind to the GAG polyelectrolyte with high affinity. At 37 °C, the reaction is exothermic for both peptides, but the amount of reaction enthalpy is about 40% larger for WR_9 (Table 1). The microscopic dissociation constant ($K_{D,i}$) is ∼100 nM for both peptides (Table 2). For statistical reason,[39] the first binding site on the GAG polyelectrolyte (i.e., at "nonsaturating conditions") has an even lower dissociation constant of $K_{D,1} = K_D/n$, where n = number of binding sites. The entropy change $T\Delta S^0$ is small compared to the reaction enthalpy (Table 1), so that the free energy of binding is mainly enthalpy-driven for both CPPs at 37 °C. The binding constant of PEG−WR_9 is by a factor of 1.8 smaller than that of the non-PEGylated WR_9. This is primarily a consequence of the different reaction enthalpies which cannot be compensated by the entropy gain of the reaction. The GAG binding results in an entropy loss for WR_9, but entropy gain for PEG−WR_9. The ∼2-fold lower binding constant was taken into account in setting up the subsequent cell culture experiments where an equal degree of GAG binding will be expected only at a 2-fold higher concentration of PEG−WR_9 as compared to WR_9.

Based on the molecular weight and sulfur content of heparin, a total of 83 negative charges per molecule are estimated (Table 1). The ITC experiments lead to a stoichiometry of about 8 CPPs per heparin. As each CPP carries a nominal charge of $z_{CPP} = +9.6$, the condition of charge neutralization is only approximately fulfilled. We have also performed ITC experiments at 17 and 27 °C and found that the reaction enthalpy of both peptides became more negative at lower temperatures. The molar heat capacity change is positive with ΔC_P^0 = 122 cal/(mol K), indicating a predominantly electrostatic binding of the CPPs to heparin (Table 2). Finally, the observed difference in entropy between the two CPPs indicates different hydrodynamic changes during GAG binding, such as different counterion release or hydration changes.

WR_9, Not PEG−WR_9, Produces GAG Aggregation. WR_9 binding to heparin produces large colloids that are easily recognized by the eye as a turbid dispersion. DLS measurements indicate a particle diameter of 300−1200 μm (Figure 3) already after the first injection of the GAG, with the largest aggregates being found at a molar ratio close to charge neutralization. In contrast, no visible aggregates were detected during GAG binding to PEG−WR_9. DLS measurements suggest a slight size change but the hydrodynamic diameter of the reaction complex remained smaller than 12 nm (Figure 3).

Table 1. Thermodynamic Parameters for Heparin Binding of WR_9 and PEG−WR_9 as Measured with ITC at 37 °C in 20 mM Tris, 100 mM NaCl, pH 7.40[a]

ligand	net charge,[b] z_{CPP}	$K_{D,i}$[c] (nM)	n binding sites per heparin[d] ($n_{CPP}/n_{heparin}$)	nz_{CPP}	reaction enthalpy, ΔH^0_{CPP} (kcal/mol CPP)	entropy, $T\Delta S^0_{CPP}$ (kcal/mol CPP)	heat capacity change,[e] $\Delta C_P{}^0_{CPP}$ (cal/(mol CPP K))
WR_9	+9.6	60 ± 11	8.15 ± 0.40	73.4 ± 3.63	−11.7 ± 0.63	−1.42 ± 0.64	122.2
PEG−WR_9	+9.6	108 ± 21	7.71 ± 0.17	69.4 ± 1.5	−8.44 ± 0.18	1.45 ± 0.26	127.9

[a] Results are reported as mean ± standard deviation from six individual measurements. [b] Net charge is calculated with respect to the amidated C-terminus of the CPPs, experimental pH of 7.4, pK_a of ∼12 for arginine's side chain, and a pK_a of 7.5 for the peptide's α-amino group in polypeptide chains.[89] [c] Microscopic dissociation constant ($K_{D,i}$) for every individual binding site (n) in a heparin chain. [d] Stoichiometry as experimentally determined for 100% of heparin's multiple binding sites (n) saturated with the specific CPP. Heparin had a sulfur content of 12.4 (w/w %) yielding 2.3 sulfate groups per average disaccharide or totally 83 negative charges per average molecule. [e] Molar heat capacity change at constant pressure ($\Delta C_P{}^0$) as calculated from the slope of ΔH^0_{CPP} as a function of three different temperatures (17, 27, and 37 °C).

Table 2. Quantification of Cellular CPP Uptake and Cell Viability by FACS[a]

	WR_9 (2 μM)	WR_9 (10 μM)	PEG−WR_9 (2 μM)	PEG−WR_9 (10 μM)
CPP	3723 ± 390	14459 ± 489	1887 ± 45	2562 ± 73
SYTOX Green	6346 ± 946	13487 ± 565	1208 ± 44	1198 ± 53

[a] Results are reported as geometric mean of the fluorescence intensity of the two dyes from three individual measurements (mean ± standard deviation). For experimental details and one raw data set, see Figure 7.

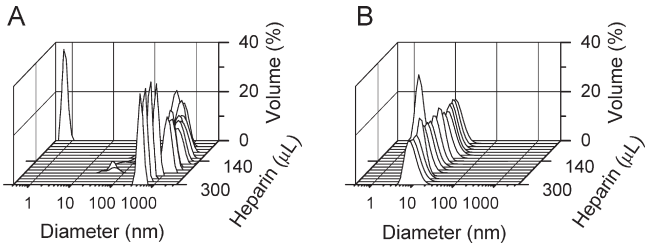

Figure 3. Particle size distribution (volume-weighted) of the GAG−CPP complexes. Dynamic light scattering of a CPP solution (1.4 mL, 60 μM) titrated with indicated volumes of heparin (100 μM, M_r ∼ 13 000)—concentrations and molar ratios that are identical to ITC titrations (Figure 2). Neutralization of formal charge is achieved for an injection volume of V_i = 150 uL of heparin (100 μM, M_r ∼ 13 000). (A) The interaction of heparin with WR_9 leads to large aggregates (0.3−1.2 μm diameter) that sediment over time (30−60 min) in the absence of stirring. (B) The interaction of heparin with PEGylated WR_9 does not produce aggregates, and the particle diameter is 2 orders of magnitude smaller with D_H = 9.3 nm. T is 25 °C, and buffer is 20 mM Tris, 100 mM NaCl, pH 7.4.

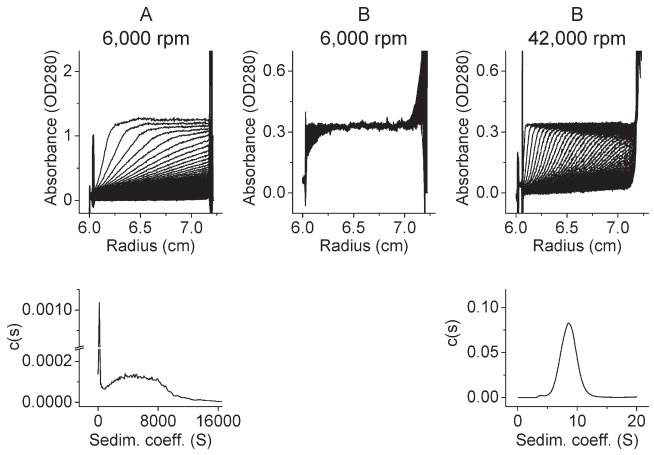

Figure 4. Analytical ultracentrifugation (AUC) of the GAG−CPP complexes. The AUC sample cell (path length 1.2 cm) contains 0.4 mL of a mixture of 600 μL of CPP (60 μM) and 96 μL of heparin (100 μM; M_r ∼ 13 000). The concentrations are equivalent to the ITC injection number 31. Upper row shows raw data of concentration distributions scanned every 1 and 5 min at 6000 or 42 000 rpm, respectively, for 8 h. Lower panel shows the sedimentation coefficient distributions using a $c(s)$ model. (A) Interaction of heparin with WR_9 leads to large and polydisperse aggregates that rapidly sediment at 6000 rpm with 84.9% of the particles having a sedimentation coefficient between 300 and 16 000 S. Because of the increased light scattering of the large particles, the OD_{280} is higher than found for the peptide alone (OD_{280} = 0.341/1.2 cm). (B) Interaction of heparin with PEGylated WR_9 forms small molecular complexes that are not meniscus-depleted at these conditions (8 h at 6000 rpm); instead, they require a much higher speed (42 000 rpm) for sedimentation. The resulting sedimentation coefficient is 2 orders of magnitude smaller (8.7 S). T is 20 °C, and buffer is 20 mM Tris, 100 mM NaCl, pH 7.4.

These different hydrodynamic properties were verified with analytical ultracentrifugation (AUC) where radial absorbance scans of the sample cells were performed every minute during 8 h (Figure 4A). At a relative mild relative centrifugal force (RCF) of 2903g (calculated for the cell bottom where r = 72 mm), the liquid column of 12 mm was essentially depleted from WR_9−GAG complexes already after 40 min (Figure 4A). At the very same conditions, the reaction complex of PEG−WR_9 and GAG was not sedimenting—even after 8 h of centrifugation (Figure 4B). Only at a 49 times higher RCF (142249g), the reaction complex was slowly sedimenting after 8 h, and the change of the reaction boundary over time allowed the quantification of the sedimentation velocity and the sedimentation coefficient s (Figure 4).

Evaluating the AUC data with a direct boundary fitting,[40] it was found that GAG binding to WR_9 produces large and heterogeneous particles with a median s of 5532 S. In contrast, GAG binding to PEG−WR_9 results in much smaller complexes with s = 8.6 S (Figure 4, bottom). Despite the obvious absence of aggregates, the complex between the GAG and PEG−WR_9 was larger than a single heparin chain with 8 CPPs bound (Table 1) because the sedimentation coefficient of the reaction complex (8.6 S) is larger than a single GAG chain (1.9 S, not shown) and 8 PEG−WR_9 (each 0.6 S, not shown). Similar conclusions follow from DLS data, where the diameter of the reaction complex

dx.doi.org/10.1021/bi1019429 |Biochemistry 2011, 50, 4650–4664

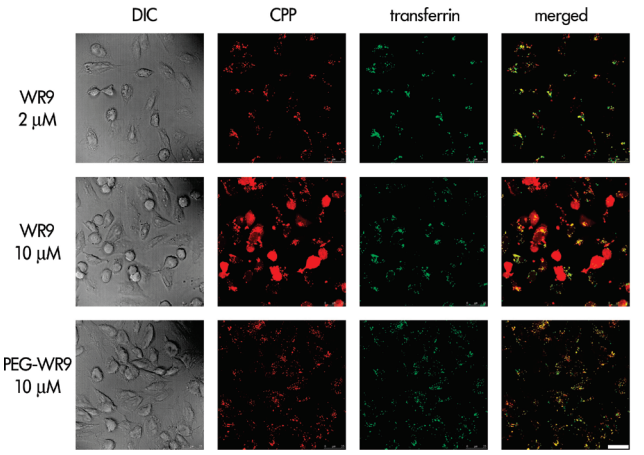

Figure 5. Colocalization of the CPP with transferrin—a marker for endocytosis. CHO-K1 cells were grown on microscope coverslips and exposed to DyLight 488-labeled transferrin (2 μM in Opti-MEM; containing antibiotics, but no FCS), followed by three times rinsing with PBS and subsequent incubation with the TAMRA-labeled CPP at indicated concentrations. After 1 h of contact time in the cell incubator, cells were rinsed three times with PBS, mounted upside down on top in 30 μL of Fluoromount G, and imaged immediately for no longer than 15 min. Colocalization of the CPP (red channel) and transferrin (green channel) results in yellow color of the merged images. White bar represents 25 μm. The results show that WR_9 shows endocytosis at <5 μM concentrations, but transduction at higher concentrations. In contrast, PEGylattion of the CPPs inhibits its capacity for transduction.

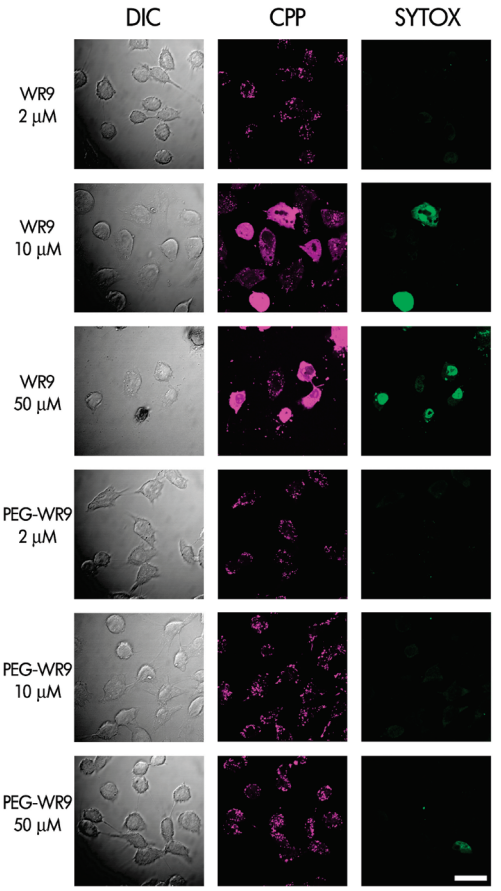

Figure 6. Colocalization of the CPP with SYTOX Green—a marker for membrane defects. CHO-K1 cells were grown on microscope coverslips and incubated with TAMRA-labeled CPPs (purple channel) at indicated concentrations. After 1 h of contact time in the cell incubator, cells were rinsed three times with PBS and then exposed to SYTOX Green (10 μM) for 10 min. Thereafter, the cells were rinsed three times with PBS, mounted upside down on top in 30 μL of Fluoromount G, and imaged immediately for no longer than 15 min. In the case of leaky membranes, SYTOX Green (green channel) experiences a signal amplification upon interaction with intracellular DNA/RNA. The white bar represents 25 μm. It is found that transduction of WR_9 leads to a general membrane instability as evidenced by uptake of SYTOX Green. In contrast, PEGylation of the CPPs inhibits both transduction and leakage of SYTOX Green.

(9.3 nm) at saturation exceeds the size of a single GAG (2.3 nm) and 8 PEG−WR_9 molecules (each 1.3 nm). This suggests that the reaction complex likely consists of ~3 GAG molecules with 3 × 8 CPPs bound. The inherent polydisperse nature of GAGs prevents a more precise quantification of the macromolecular assembly.

Concentration-Dependent Cellular Localization of WR_9. Knowing that PEGylation prevents the GAG clustering, but not GAG binding, we tested whether the glycan clustering affects the uptake of the CPP on living cells in culture. To this purpose, both CPPs were fluorescently labeled at the N-terminus using TAMRA.

Living CHO-K1 cells were exposed for 1 h to 2 μM TAMRA-labeled WR_9, where smaller peptide aggregates were detected at the cell surface. In order to identify the only small amounts of intracellular CPP, the extracellular CPP was removed by rinsing the cells with buffer and heparin which removes the cell-surface bound CPP.[21] The cells were imaged instantly, and a punctuate fluorescent staining was observed within the cells (Figure 5). This punctuate staining suggests an endocytic uptake of the CPP. The endocytosis was confirmed by colocalization with fluorescently labeled transferrin (Figure 5, upper row). Transferrin is an iron-binding protein (M_r ~ 79 550) being routed to endosomes. Its specific interaction with the glycosylated transferrin receptor mediates a cytoplasmic receptor phosphorylation and subsequent formation of clathrin coats.[41] Transferrin is thus used as a marker of clathrin-mediated endocytosis.

In contrast, at higher concentrations (>5 μM), TAMRA-WR_9 was no longer confined to endocytic vesicles but was found to be spread diffusively over cytoplasm and nucleus in approximately half of the cell population (Figure 5, middle row). In these cells, the fluorescence intensity at identical photomultiplier settings was much higher than found for endocytic CPP uptake, suggesting a massive influx of the CPP into cytosol and nucleus. This indicates either the cytoplasmic or the endosomal membrane was leaky to the nonamphipathic CPP at concentrations of >5 μM. The rapid access to the cytosol has been previously termed "transduction"[28] and has led to many different hypothesis on the physical basis of the CPP-induced bilayer instability. As a consequence of the membrane damage in present experiments, the membrane became permeable to the vital stain SYTOX Green which was found specifically in all cells showing CPP transduction (Figure 6). At even higher concentrations (>50 μM for 1 h), 1−2 cells per field of view became necrotic with visible cell shrinkage and condensation of chromatin (Figure 6). Similar necrotic effects are known from cationic lipofectants at elevated concentrations.[42]

Only Endocytosis for PEG−WR_9. Next we tested the cellular uptake of PEGylated WR_9. TAMRA-labeled PEG−WR_9 was

dx.doi.org/10.1021/bi1019429 |*Biochemistry* 2011, 50, 4650–4664

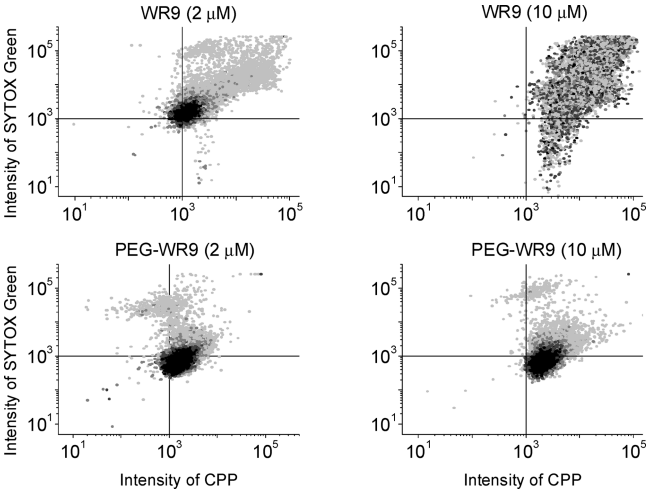

Figure 7. FACS data (density plots) for cellular CPP uptake and viability of 10 000 cells. CHO-K1 cells were grown in 6-well culture flasks and were incubated with TAMRA-labeled CPPs at indicated concentrations. After 1 h of contact time with the CPP in the cell incubator, cells were rinsed three times with PBS and then exposed for 10 min to SYTOX Green (10 μM)—a marker for membrane defects. Thereafter, the cells were rinsed three times with PBS, detached with Accutase, and washed twice with heparin and PBS to remove superficially bound CPPs. The fluorescence intensity of the CPPs and SYTOX Green was measured in 10 000 CHO cells using FACS with same photomultiplier settings allover. It is found that transduction of WR_9 at 10 μM leads to a general membrane instability as evidenced by the increased uptake of SYTOX Green. In contrast, PEGylation of WR_9 inhibits both its enhanced uptake and uptake of SYTOX Green.

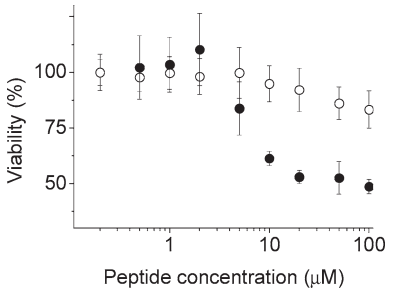

Figure 8. Viability of CHO-K1 cells after exposure to different CPP concentrations. The CellTiter 96 aq assay measures production of a colored formazan product as result of functional cell metabolism. Cellular metabolism is measured after a 1 h exposure to different CPP concentrations of (●) WR_9 and (○) PEG−WR_9 and is reported with respect to untreated cells as a control. Results are reported as mean ± standard deviation from eight individual measurements.

applied to CHO cells at a concentration of up to 50 μM, which more than compensated its 2-fold lower binding constant compared to WR_9 showing transduction at >5 μM concentration. The experimental results are shown in Figures 5 and 6. TAMRA-PEG−WR_9 always produced a punctuate intracellular cell staining that overlaid well with endocytic transferrin uptake (Figure 5). We therefore conclude that PEG−WR_9 is taken up by CHO cells only via the endocytotic route. These microscopic observations on the subcellular distribution of the CPP were corroborated in whole cell extracts, FACS, and toxicity assays which were used to quantify the CPP effects in a larger collective.

Whole cell lysates of $\sim 2 \times 10^6$ cells were analyzed for their intracellular CPP content and total protein content. Here, a 1 h incubation time with extracellular CPPs at 10 μM led to an intracellular TAMRA-WR_9 and TAMRA-PEG−WR_9 content of 2393 ± 223 and 123 ± 7 nmol CPP/mg total protein, respectively (n = 8). The 19.5-fold higher intracellular CPP content indicates that transduction of WR_9 is much more efficient than endocytosis of TAMRA-PEG−WR_9, substantiating microscopic findings of intense intracellular staining after WR_9 transduction and low microscopic intensity with PEG−WR_9.

Likewise, FACS measurements (Figure 7 and Table 2) confirmed the much higher WR_9 uptake by transduction. In a first series of experiments, cells were exposed to a 2 μM extracellular CPP concentration—conditions where microscopic observations indicated primarily endocytic uptake for both CPPs (Figures 5 and 6). At this concentration, the FACS experiments showed that the CPP uptake of both CPPs differed by a factor of only 1.97 (Table 2), which might reflect the weaker affinity of PEG−WR_9 for GAGs and/or some transduction of WR_9 already at that low concentration. At higher extracellular CPP concentration (10 μM), however, the CPP uptake became much more pronounced for WR_9 as compared to PEG−WR_9 (Table 2), supporting the microscopic observation where transduction of WR_9 led to higher intracellular CPP contents than endocytosis with PEG−WR_9 at equal extracellular concentration.

We find that transduction of WR_9 perturbs both the membrane stability and the metabolic activity of the cells. CHO cells that show WR_9 transduction also show an increased membrane permeability to SYTOX Green—a cationic cyanine dye that usually cannot cross intact cell membranes unless they are damaged (Figure 6). These microscopic findings of increased SYTOX Green membrane permeability were confirmed by dual staining experiments in FACS, where the increased WR_9 uptake was paralleled by the increased uptake of SYTOX Green (Figure 7). It is known from literature that SYTOX Green shows a >500-fold enhancement of fluorescence emission when bound to intracellular nucleotides, so that this assay is more sensitive than viability tests using propidium iodide.[29]

Higher Toxicity for WR_9. These adverse effects of WR_9 transduction are further confirmed in present study using a metabolic assay where WR_9 transduction reduced the metabolic activity of the cell population up to 50% (Figure 8). It is noteworthy that the dose−response curve did not reveal a typical decay to 0% at highest peptide concentration. This supports the microscopic findings of two cell populations where only about 50% of the cells show WR_9 transduction (Figures 5 and 6). The differences between the different cell populations might be the result of cell-cycle related shedding of cell-surface adhesion molecules[43] and extracellular matrix remodeling that both appear to be required for CPP transduction. Not only the CPP concentration (Figures 6−8) but also the contact time seems to be important for toxicity because it was found previously that transduction of 100 μM HIV-1 Tat-PTD during much shorter time (<5 min) did not lead to membrane defects,[29] which must be further investigated prior to applications of WR_9 in larger organisms.

Vector Efficiency. As a measure of their transport capacity, we have analyzed the CPP-mediated transient transfection of CHO-K1 cells with the plasmid for enhanced green fluorescent protein (gWIZ GFP). Equal N/P ratios of 2 were used for the CPPs, resulting in cationic polyplexes, and the CPPs were compared with a commercial transfection kit (Lipofectamine2000). The

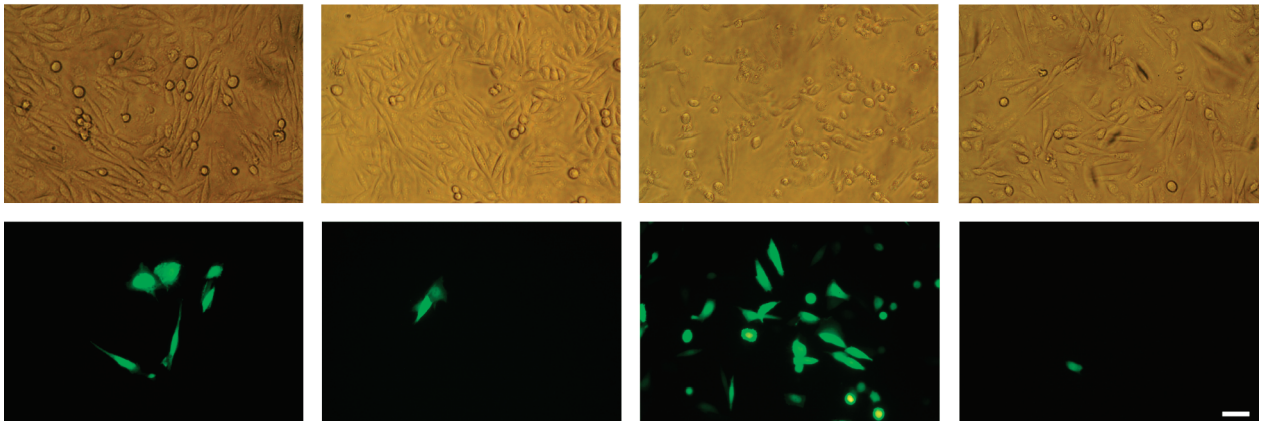

Figure 9. Transfection of CHO-K1 cells with gWIZ-GFP. CHO-K1 cells were grown in plastic wells to ~90% confluency, exposed to the vector/plasmid polyplex (N/P = 2 and 3 for CPP and lipofectant, respectively) for 1 h, and recorded after 24 h of protein expression. Bright-field (upper row) and fluorescence views of GFP expression (lower row) were taken directly from the plastic dishes of the cell culture using an inverted microscope. From left to right: 10 μM WR_9, 10 μM PEG−WR_9, 3.5 μM Lipofectamine, and plasmid only. The GFP fluorescence intensity per well was 345 ± 30.4, 52.1 ± 16.6, 1082 ± 77.1 and 8.1 ± 0.4 RLU for WR_9, PEG−WR_9, Lipofectamine, and plasmid only (n = 8 wells per compound; similar cell count).

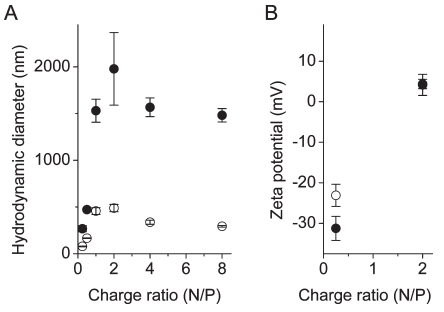

Figure 10. Hydrodynamic properties of the plasmid−CPP complexes. (A) Dynamic light scattering of a gWIZ-GFP solution (130 μL; 50 μM as dinucleotide) containing the CPPs at concentrations from 3 to 89 μM, corresponding to a charge ratio (N/P) from 0.25 to 8, respectively. Largest particle size is observed close to charge neutralization and leads to sedimentation of the complexes for WR_9. In contrast, the PEGylation significantly reduces the particle size. (B) Same experiments in a larger volume (1.3 mL) in order to measure the zeta potential of the colloids. Data show average and standard deviation from three preparations. T is 25 °C, and buffer is 20 mM Tris, 100 mM NaCl, pH 7.4. WR_9 (filled symbols), PEG-WR_9 (open symbols).

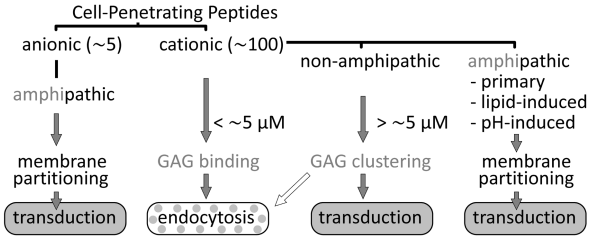

Figure 11. Current understanding of CPP uptake routes. Depending on the structural property of the CPP and its resulting affinity for diverse membrane constituents (e.g., lipids and glycans), several competing cellular uptake routes exist, where the extracellular CPP concentration is essential. Adsorptive endocytosis is mainly provided by GAG binding of the CPP, but other anionic cell-surface glycans, such as sialylated glycans, can substitute GAGs. Structural properties of the CPP and cargo, such as size, regulate what type of endocytosis is prevailing (e.g., macropinocytosis, clathrin-mediated). Largest GAG clustering propensity is observed at formal charge neutralization of the GAG, so that the indicated concentration for transduction presumably varies among different CPPs, glycans, and cell types. When using chromophores to trace the fate of the CPP, the transduction typically leads to diffuse staining of the cytosol (indicated by dotted box), whereas endocytosis yields a punctuate staining of small endocytic vesicles (indicated by plain gray boxes).

CPPs were used at a 10 μM extracellular concentration (9 cations/CPP) where transduction is observed for WR_9, but only endocytosis for PEG−WR_9. Cationic Lipofectamine was used at 3.5 μM concentration (5 cations/DOSPA) as recommended by the supplier. Lipofectamine was used in its factory-optimized formulation including additives such as DOPE—in contrast to the CPPs that were used without helper additives. Although CHO cells are in general more difficult to transfect than other adherent cell lines, present results show that higher GFP expression was achieved with WR_9 as compared to PEG−WR_9 or the plasmid only (Figure 9). On the other hand, transfection with the optimized commercial transfection kit was even more efficient as evident from both the higher GFP intensity per cell and the number of cells showing GFP expression (Figure 9). Analysis of the particle size (Figure 10) reveals that the CPP−plasmid complexes are much larger than the free CPP in solution (Figure 3). Largest particle size was found close to charge neutralization. In view of the potential effect of the particle size on the uptake,[30] it would be interesting to investigate whether these aggregates and free CPPs differ in their cellular uptake properties. In analogy to the CPP−GAG complexes, the PEGylation of WR9 considerably reduced the size of the complexes at all charge ratios tested (Figure 10). The zeta potential of the colloids was slightly reduced by the PEGylation (Figure 10). In this respect, it has been reported previously that PEGylation moves the shear plane of charged colloids away from the surface as a function of PEG length and density thus reducing the zeta potential.[44]

DISCUSSION

We have synthesized two CPPs that allow us to identify and distinguish two different uptake pathways of CPPs, namely endocytosis and transduction. We conclude from present results and current literature that there is not a single, but distinct,

cellular uptake route for the structurally different CPPs—despite their common name. A schematic summary of possible pathways is given in Figure 11, which will be discussed in more detail below. Especially the transduction of nonamphipathic CPPs is one of the least understood biological pathways at present which can be hardly explained by invoking a purely lipid bilayer as entry gate.

We find that the biological uptake of PEG−WR_9 proceeds only via endocytosis. In contrast, the biological uptake of WR_9 is more complex and follows two different pathways, namely (i) endocytosis and (ii) an additional, more efficient pathway termed transduction. We show that transduction proceeds via the GAG clustering capacity of WR_9 and is inhibited when clustering is blocked by PEGylation. Especially transduction is of foremost interest in biotechnology because it provides a higher and faster access to cytosol and cell nucleus as compared to endocytosis (Figure 5).

Figure 11 then demonstrates that different pathways may be used depending on the chemical nature and concentration of the CPP. Some CPPs have amphipathic properties and may act in a detergent-like manner. In experiments with pure lipid membranes, they will easily translocate across the lipid barrier. This is not the case for the highly cationic WR_9 which cannot pass a purely lipid barrier.[25] On the other hand, when exposed to intact biological membranes, such as CHO cells, uptake of WR_9 into the all interior can occur at different levels of efficiency. By comparing WR_9 with its analogue PEG−WR_9, we succeeded in differentiating two different pathways. The transduction of PEG−WR_9 is hindered by its brushlike $-(CH_2CH_2O)_{27}-$ extension preventing the link with a larger number of glycosylated proteins even though it binds almost as strongly to sulfated GAGs as the non-PEGylated WR_9. The uptake of PEG−WR_9 proceeds exclusively by endocytosis as evidenced by its colocalization with the endocytic marker transferrin. In contrast, the smaller CPP WR_9 can be imported not only by endocytosis but also by transduction. We find that the uptake of WR_9 via transduction depends on glycan binding and glycan clustering and that the concentration of WR_9 controls the uptake route and the subcellular distribution of the CPP.

Adsorptive Endocytosis. At low micromolar extracellular CPP concentration (<5 μM), we find that both CPPs (WR_9 and PEG−WR_9) are taken up into endocytic vesicles, and there is little, if any, CPP release into the cytosol, at least for the specific conditions used (cell type, cell density, and time window). Several studies since 1965 have suggested that the endocytic uptake of similar polyamines requires the tight, but unspecific, binding to anionic cell-surface glycoproteins and glycolipids.[5,16,20,45] In this adsorptive-mediated endocytosis, the anionic glycan moiety is essential because its enzymatic removal or competition with externally added glycans reduces or even abolishes the polyamine uptake.[16−18,29] In support, it is known that the cationization of larger proteins, such as albumin and immunoglobulins, strongly enhances their endocytic uptake.[46] On the other hand, the increased uptake via adsorptive endocytosis provides not necessarily access to compartments that support transcription of the cargo.[47−49]

In experiments using cationized albumin, adsorptive endocytosis has been characterized by half-saturation concentration of ~0.8 μM,[50] which is much higher than that of receptor-mediated endocytosis (e.g., 2.2 nM for EGF[51]). The present FACS data show that the uptake of PEG−WR_9 is not even saturated at a 2-fold higher concentration, i.e., 2 μM CPP (Table 2), supporting an uptake via adsorptive endocytosis rather than receptor-mediated endocytosis. This is further supported by confocal microscopy. Intracellular uptake of TAMRA-WR_9 and TAMRA-PEG−WR_9 was only observed when the extracellular CPP concentrations were above 20 and 50 nM, respectively, at a maximum photomultiplier gain of the microscope, specific plane thickness of 0.7 μm, and a 1 h contact time with the CPP. These minimum concentrations are in agreement with the K_D values measured with ITC for the interaction of the CPPs with the GAG heparin (Table 1) and suggest a tight binding of the two CPPs to sulfated GAGs at the membrane surface.

At 2 μM extracellular concentration, the amounts of endocytic PEG−WR_9 and WR_9 uptake are similar (Table 2). The similarity in their endocytic uptake suggests that the cell surface binding of the polyamines provides a common basis for their adsorptive endocytosis. It is currently unknown whether this binding to cell-surface glycans provides an active endocytic *signaling* like in receptor-mediated endocytosis or whether adsorptive endocytosis is agonist-independent, exploiting passively the constitutive membrane flow[52] and rapid turnover of proteoglycans[53] proceeding at a fraction of the cell cycle.

The pronounced colocalization with transferrin suggests that a major portion of the WR_9 and PEG−WR_9 uptake at concentrations <2 μM proceeds via clathrin-mediated endocytosis. The caveolae-mediated type of endocytosis seems to be optimal to avoid the degradation in the lysosome.[54,55] In more general terms, the endocytic CPP uptake appears to be a mix of clathrin-coated endocytosis,[56] macropinocytosis,[31,57] caveolae,[32] and clathrin/caveolae-independent endocytosis.[58] The cargo size[45] and other vector properties can influence the relative contribution of these pathways and the consequences for cargo degradation and activity. The tight interaction with proteoglycans may lead to a competitive release of electrostatically bound potential cargos.[59]

In contrast, shorter amines such as natural putrescine ($Z = +2$) and spermidine ($Z = +3$) accumulate in the cytosol at millimolar concentrations[60] through the action of specific transmembrane transport proteins ($K_m \sim 0.2-390$ μM).

At concentrations <5 μM, the two tested CPPs remain localized in endocytic vesicles. Because of the sensitivity limits in confocal microscopy, we cannot exclude that *minute* fractions of the CPP might have escaped from endocytic vesicles to the cytoplasm. Such minute fractions could be detected with more sensitive techniques such as gene expressing CPP-Cre assays,[18,30] but they are in no way comparable to the massive WR_9 transduction observed at higher CPP concentrations (see below). Potential therapeutic applications of CPPs thus depend critically on the number of cargo molecules that are required in the cytosol or in the nucleus to produce their effect. From virology, it is known, for example, that a single virus particle can be sufficient to infect a cell.[61] Hence, a few molecules escaping from the endocytic vesicles into the cytosol may be sufficient for biological purposes even though they cannot be detected with current microscopic techniques.

Transduction. We observe that WR_9 can easily translocate into the cytosplam and nucleus in ~50% of the cells ("transduction") when the extracellular concentration of WR_9 exceeds 5 μM. The transduction of WR_9 leads to a 19.5-fold increase of the intracellular CPP content in whole cell lysates as compared to the endocytic uptake of PEG−WR_9 when compared at 10 μM extracellular CPP concentration. In contrast, PEG−WR_9 is only restricted to endocytic uptake without signs

for transduction even when increasing the extracellular concentration to 50 μM (Figure 6). This suggests that the transduction of WR_9 results either from an uptake route independent of endocytosis or by an unusually enhanced endocytosis with additional endosome release. The concentration-dependent change from endocytic CPP uptake to transduction was observed in adherent cells. Our observations thus support previous reports on cells in suspension[62] that differ from adherent cells with regard to agglutination and cell hybridization upon polycation binding.[63,64]

Related gene expression studies[18,30] and careful confocal microscopy studies have shown indeed that the polyamines have substantial access to the cytosol and nucleus,[29,65−67] suggesting the instability of the plasma and/or endosome membrane to the CPP and eventual cargo. Whereas membrane leakage of pH-sensitive peptides[68] and PEI[69] has been proposed to proceed at the level of the endosome membrane, it has been concluded that the transduction of nonamphipathic CPPs involves mainly the plasma membrane.[32,65] Our results support this later hypothesis because the total intracellular CPP content at equal extracellular CPP concentration was 19.5-fold higher for transduction of WR_9 as compared to endocytosis of PEG−WR_9. In contrast, a rapid endosomal escape of WR_9 would change its intracellular distribution, but not necessarily the intracellular content. Moreover, the rate of CPP transduction has been reported to be ∼20 times faster[29] than known typical escape rates from the endosome.[70] We and others have previously shown that the transduction of nonamphipathic CPPs at high micromolar concentrations coincides spatially and temporarily with the clustering of the polyamines at the cell surface.[29,71−74] Present results strengthen these observations because they provide evidence for transduction being inhibited, when GAG clustering is hindered by sterically unfavorable CPPs. On a molecular basis, the physical forces driving the transduction after the cell-surface capping are not known so far, but the observed extracellular matrix deformations may enhance the permeability of the membrane.[75] In this regard, observations on CPP-related compounds suggest that such dense aggregates on the cell surface destabilize the membrane by a multilayered process affecting mechanical curvature stress,[76] local dehydration,[77] hydrophobic mismatch,[78] lipid scrambling,[79] and resealing defects.[80] The transduction of nonamphipathic CPPs is thus enhanced by nonbilayer forming lipids[81] that increase the bending rigidity of membranes by altered acyl chain packing and by promotion of nonbilayer structures.

Beside the capacity for GAG clustering, the two CPPs differ also in their molecular size by a factor of 1.8. A much larger cargos size was reported to shift the uptake of CPPs among various endocytosis subtypes.[20] Therefore, it might be possible that not only the concentration and different GAG clustering propensity contribute to the transduction, but also the smaller size of WR_9 (M_r = 1609) as compared to PEG−WR_9 (M_r = 2914). On the other hand, the transduction of nona-arginine was similar to the larger icosa-arginine (M_r = 3142), i.e., a size match to PEG−WR_9 (M_r = 2914).[33] Also, the coupling of a 120 kDa enzyme to Tat-PTD did not abolish its transduction and activity in the cytosol.[28] In view of potential hydrophilic differences, the octanol−water partition coefficient was unchanged when coupling a short PEG chain (M_r = 3400) to an arginine-rich peptide.[82]

Thermodynamic Considerations. Despite the large difference in their biological uptake, we find that WR_9 and PEG−WR_9 have a similar high affinity for the GAG heparin that is a structural analogue of cell-surface heparan sulfate. Using ITC, DLS, and AUC, we find that WR_9 binds to the GAG at submicromolar concentrations (Table 1), which is thus relevant to the biological CPP uptake observed at these concentrations. The ITC experiments demonstrate that the interaction of WR_9 with the GAG is mostly enthalpy driven (Table 1), which is rather surprising as electrostatic interactions are commonly associated with positive entropy changes through release of water and monovalent counterions.

Because of their multiple binding sites, CPPs and GAGs can produce multimolecular interactions that lead to electrostatic cross-linking ("clustering"). We observe that WR_9 and heparin form large colloidal aggregates upon binding. The aggregate size was found to be largest close to charge neutralization. The size and morphology of such complexes are influenced by the kinetics[83] and the order of mixing.[84] An additional excess of ligand might lead to redissolution ("overcharging") of the complex, but the concentration threshold for redissolution has been reported to be 2 orders of magnitude higher than that observed for saturation.[85] Aggregate formation upon GAG binding is abolished if WR_9 is PEGylated. The PEG brush apparently inhibits the cross-linking of surface molecules.

As a peculiarity, we observe small endothermic contributions close to charge neutralization which indicates a reorganization of the CPP−GAG complex at saturating conditions. Such slow kinetic responses have been reported for polyelectrolyte overcharging,[83] and the small endothermic contribution might also explain the finding that the binding affinity increases with temperature despite its exothermic nature.[86] When continuing the titration beyond charge neutralization, the excess of the ligand no longer produced substantial changes in size (Figure 3) or heat flow (Figure 2), suggesting that redissolution of the complex was not achieved even at a 2-fold excess charge.

The size of the WR_9−GAG aggregates approaches the low micrometer range (Figure 3), suggesting a potential clotting risk in blood capillaries and also impeding measurements with optical techniques. PEGylation of the CPP would reduce this risk and potential physiological side effects, although the high affinity for GAGs is maintained. The binding of PEG−WR_9 is driven by a favorable negative enthalpy change but, in contrast to WR_9, also by a favorable positive entropy change. The inhibition of the GAG clustering is thus likely a consequence of steric hindrance, where the length of the PEG brush restricts the formation of intermolecular interactions.

Whereas the low concentration of covalently bound PEG (<100 μM) inhibited the transduction of WR_9 into CHO-K1 (Figure 4), it is also known that much higher PEG concentrations can produce quite the opposite effect. For example, 10−50% (m/m) of free PEG in cell growth media leads to enhanced membrane fusion and cell agglutination as consequence of high osmolality and local dehydration of the membrane.[87]

Toxicity. We find that the concentration required for WR_9 transduction (Figure 6) affects both the cellular metabolism (Figure 8) and membrane leakage to SYTOX Green, which are both signs of cell toxicity. It thus can be argued that transduction of nonamphipathic CPPs is paralleled by a membrane damage which leads to a rather narrow therapeutic windows as known from cationic lipofectants. For example, an efficient transfection with the pentavalent lipofectamine requires a concentration of >6.8 μM, whereas a lethality of >90% was observed at a only 5 times higher concentration (34 μM) for several cell lines.[42]

It is thus critical to review CPP concentrations used in previous research in order to clarify whether endocytosis or

transduction is relevant for optimum cellular response of transported cargos. The early studies with CPPs employed concentrations of 10 μM Tat for 8 h[7] to obtain efficient plasmid expression — especially when no helper molecules, such as chloroquine, were added. Our results indicate that not only endocytosis but also transduction is expected at these conditions. In the present study, we also find that WR_9 transduction produced more GFP expression than WR_9 endocytosis (Figure 9). This suggests that, in analogy to lipofectants, nonamphipathic CPPs, such as WR_9 and Tat, are most effective at concentrations where they produce transduction, but are not yet irreversibly toxic. The concentration for cell damage might be reduced in the presence of electrostatically bound cargos because of the reduction of the overall charge of the complex.

Surprisingly, WR_9 did not damage 100% of the cells in present experiments. In contrast to typical dose−response curves, WR_9 reduced the cellular metabolism to only 50% of the population in the specific concentration range. Similar results were found in microscopy, where both CPP and SYTOX Green leakage was observed in only 50% of the cells. This distinct response of apparently two cell subpopulations indicates that WR_9 transduction might be specific to cell-surface molecules that are expressed at certain stages of the cell cycle or cell side.[88] Another explanation might be the unspecific membrane instability to macromolecules during mitosis,[43] but in this case, PEG−WR_9 should have also shown transduction.

Although the mechanism of the polyamine toxicity is not well understood, it is likely that it also proceeds via cell surface capping. It has been reported that the length of the polycation is more critical to its toxicity than the extent of its surface binding.[73] Using a 5 min incubation time with HIV-1 Tat-PTD, it was shown that the membrane damage at CPP concentrations <100 μM is reversible after 5 min exposures.[29] Similar results on low toxicity of short-term CPP exposures were also reported in other toxicity studies.[26] Recovery from transient CPP exposure is also evident from numerous studies reporting successful gene expression and thus an active cell machinery for transported cargo plasmids.

For application in organisms, an additional toxicity might arise from the aggregation of the multivalent vectors with blood constituents. For example, red blood cell agglutination, complement activation, aggregation with blood albumin, and resulting risks for emboli have prevented the use of poly-L-lysine as medical transfectant in the 1960s and 1970s. Because of a structural analogy, similar problems might be expected for nonamphipathic WR_9 at micromolar concentrations. In this respect, we show that PEGylation of the CPP with 27 ethylene oxide repeats is sufficient to prevent the aggregation with the anionic GAG and thus to reduce the toxicity of the CPP.

CONCLUSIONS

We have shown that transduction and endocytosis provide two distinct routes for CPP uptake into living cells. Amphipathic CPPs, such as penetratin p2AL, induce transduction even in model membranes by insertion into and perturbation of the lipid membrane. This pathway is not possible for highly charged, nonamphipathic CPPs, such as WR_9 (Figure 11), suggesting additional molecules being involved such as anionic cell-surface molecules (e.g., GAGs).

We find that the cellular uptake of WR_9 into CHO cells switches from endocytosis to transduction at concentrations >5 μM. Within a few minutes, transduction provides a high concentration of WR_9 in the cytosol and nucleus of CHO cells which might be favorable for biomedical purposes. On the other hand, transduction impairs the cell membrane integrity and thus the cell viability over time. Therefore, the reversibility of the cellular changes might limit the therapeutic applicability of CPPs— in close analogy to the known cytotoxicity of related lipofectants.

In contrast to WR_9, its PEGylated variant (PEG−WR_9) showed only endocytic uptake and only negligible toxicity, but no longer the rapid transduction into the cytosol and nucleus. This entrapment of PEG−WR_9 in endocytic vesicles and the subsequent degradation of the vesicle content appear of minor therapeutic relevance as compared to the transduction of WR_9— unless combined with endosomolytic drugs.

Comparing the different cellular uptake properties of WR_9 and PEG−WR_9, we find that PEGylation of WR_9 prevents the CPP aggregation with GAGs, but not its GAG binding. We therefore conclude that GAG binding provides CPP uptake via adsorptive endocytosis. In contrast, the aggregation of WR_9 with cell-surface molecules destabilizes biological membranes by an additional, multilayered process leading to transduction.

AUTHOR INFORMATION

Corresponding Author

*Phone: 41-61-2672180. Fax: 41-61-2672189; E-mail: andre.ziegler@unibas.ch.

Funding Sources

This work was supported by the Swiss National Science Foundation under Grant No. 3100-107793/1.

ACKNOWLEDGMENT

Beatrice Muller (Department of Infection Biology) provided excellent support during the FACS measurements.

ABBREVIATIONS

AUC, analytical ultracentrifugation; CPPs, cell-penetrating peptides; DLS, dynamic light scattering; FACS, fluorescence-activated cell sorting; FCS, fetal calf serum; GAGs, glycosaminoglycans; ITC, isothermal titration calorimetry; K_D, dissociation constant; M_r, relative molecular mass; N/P ratio, ratio of cationic nitrogen and anionic phosphate in mixtures of cationic transfection reagents and anionic DNA; PBS, phosphate buffered saline; PEG, poly(ethylene glycol); RCF, relative centrifugal force; WR_9, tryptophan-labeled nona-L-arginine.

REFERENCES

(1) Yildirim, M. A., Goh, K. I., Cusick, M. E., Barabasi, A. L., and Vidal, M. (2007) Drug-target network. *Nature Biotechnol. 25*, 1119–1126.

(2) Chen, S. Y., Bagley, J., and Marasco, W. A. (1994) Intracellular antibodies as a new class of therapeutic molecules for gene therapy. *Hum. Gene Ther. 5*, 595–601.

(3) Lipinski, C. A., Lombardo, F., Dominy, B. W., and Feeney, P. J. (2001) Experimental and computational approaches to estimate solubility and permeability in drug discovery and development settings. *Adv. Drug Delivery Rev. 46*, 3–26.

(4) Parsegian, A. (1969) Energy of an ion crossing a low dielectric membrane: solutions to four relevant electrostatic problems. *Nature 221*, 844–846.

(5) Ryser, H. J., and Hancock, R. (1965) Histones and basic polyamino acids stimulate the uptake of albumin by tumor cells in culture. *Science 150*, 501–503.

(6) Frankel, A. D., and Pabo, C. O. (1988) Cellular uptake of the tat protein from human immunodeficiency virus. *Cell 55*, 1189–1193.

(7) Green, M., and Loewenstein, P. M. (1988) Autonomous functional domains of chemically synthesized human immunodeficiency virus tat trans-activator protein. *Cell 55*, 1179–1188.

(8) Ziegler, A. (2008) Thermodynamic studies and binding mechanisms of cell-penetrating peptides with lipids and glycosaminoglycans. *Adv. Drug Delivery Rev. 60*, 580–597.

(9) Moulton, H. M., Fletcher, S., Neuman, B. W., McClorey, G., Stein, D. A., Abes, S., Wilton, S. D., Buchmeier, M. J., Lebleu, B., and Iversen, P. L. (2007) Cell-penetrating peptide-morpholino conjugates alter pre-mRNA splicing of DMD (Duchenne muscular dystrophy) and inhibit murine coronavirus replication in vivo. *Biochem. Soc. Trans. 35*, 826–828.

(10) Lebleu, B., Moulton, H. M., Abes, R., Ivanova, G. D., Abes, S., Stein, D. A., Iversen, P. L., Arzumanov, A. A., and Gait, M. J. (2008) Cell penetrating peptide conjugates of steric block oligonucleotides. *Adv. Drug Delivery Rev. 60*, 517–529.

(11) Regina, A., Demeule, M., Che, C., Lavallee, I., Poirier, J., Gabathuler, R., Beliveau, R., and Castaigne, J. P. (2008) Antitumour activity of ANG1005, a conjugate between paclitaxel and the new brain delivery vector Angiopep-2. *Br. J. Pharmacol. 155*, 185–197.

(12) Bates, E., Bode, C., Costa, M., Gibson, C. M., Granger, C., Green, C., Grimes, K., Harrington, R., Huber, K., Kleiman, N., Mochly-Rosen, D., Roe, M., Sadowski, Z., Solomon, S., and Widimsky, P. (2008) Intracoronary KAI-9803 as an adjunct to primary percutaneous coronary intervention for acute ST-segment elevation myocardial infarction. *Circulation 117*, 886–896.

(13) Scherrmann, J. M., and Temsamani, J. (2005) The use of Pep: Trans vectors for the delivery of drugs into the central nervous system. *Int. Congr. 1277*, 199–211.

(14) Levin, C., Fiorentino, D. F., Vosganian, G., Chon, S., and Kimball, A. B. (2003) The safety of topical cyclosporin A conjugate (CGC1072) in the treatment of mild to moderate psoriasis. *J. Invest. Dermatol. 121* (Conference Abstract), 1201.

(15) Pouton, C. W., Lucas, P., Thomas, B. J., Uduehi, A. N., Milroy, D. A., and Moss, S. H. (1998) Polycation-DNA complexes for gene delivery: a comparison of the biopharmaceutical properties of cationic polypeptides and cationic lipids. *J. Controlled Release 53*, 289–299.

(16) Mislick, K. A., and Baldeschwieler, J. D. (1996) Evidence for the role of proteoglycans in cation-mediated gene transfer. *Proc. Natl. Acad. Sci. U.S.A. 93*, 12349–12354.

(17) Belting, M., Persson, S., and Fransson, L. A. (1999) Proteoglycan involvement in polyamine uptake. *Biochem. J. 338* (Pt 2), 317–323.

(18) Wadia, J. S., Stan, R. V., and Dowdy, S. F. (2004) Transducible TAT-HA fusogenic peptide enhances escape of TAT-fusion proteins after lipid raft macropinocytosis. *Nature Med. 10*, 310–315.

(19) Wender, P. A., Mitchell, D. J., Pattabiraman, K., Pelkey, E. T., Steinman, L., and Rothbard, J. B. (2000) The design, synthesis, and evaluation of molecules that enable or enhance cellular uptake: peptoid molecular transporters. *Proc. Natl. Acad. Sci. U.S.A. 97*, 13003–13008.

(20) Rejman, J., Oberle, V., Zuhorn, I. S., and Hoekstra, D. (2004) Size-dependent internalization of particles via the pathways of clathrin- and caveolae-mediated endocytosis. *Biochem. J. 377*, 159–169.

(21) Richard, J. P., Melikov, K., Vives, E., Ramos, C., Verbeure, B., Gait, M. J., Chernomordik, L. V., and Lebleu, B. (2003) Cell-penetrating peptides. A reevaluation of the mechanism of cellular uptake. *J. Biol. Chem. 278*, 585–590.

(22) Lundberg, M., and Johansson, M. (2002) Positively charged DNA-binding proteins cause apparent cell membrane translocation. *Biochem. Biophys. Res. Commun. 291*, 367–371.

(23) Leifert, J. A., and Whitton, J. L. (2003) "Translocatory proteins" and "protein transduction domains": a critical analysis of their biological effects and the underlying mechanisms. *Mol. Ther. 8*, 13–20.

(24) Deshayes, S., Plenat, T., Charnet, P., Divita, G., Molle, G., and Heitz, F. (2006) Formation of transmembrane ionic channels of primary amphipathic cell-penetrating peptides. Consequences on the mechanism of cell penetration. *Biochim. Biophys. Acta 1758*, 1846–1851.

(25) Sauder, R., Seelig, J., and Ziegler, A. (2010) 10. Thermodynamics of lipid interactions with cell-penetrating peptides. *Methods Mol. Biol. 683*, 129–155.

(26) Saar, K., Lindgren, M., Hansen, M., Eiriksdottir, E., Jiang, Y., Rosenthal-Aizman, K., Sassian, M., and Langel, U. (2005) Cell-penetrating peptides: a comparative membrane toxicity study. *Anal. Biochem. 345*, 55–65.

(27) Henriques, S. T., Melo, M. N., and Castanho, M. A. (2006) Cell-penetrating peptides and antimicrobial peptides: how different are they? *Biochem. J. 399*, 1–7.

(28) Schwarze, S. R., Ho, A., Vocero-Akbani, A., and Dowdy, S. F. (1999) In vivo protein transduction: delivery of a biologically active protein into the mouse. *Science 285*, 1569–1572.

(29) Ziegler, A., Nervi, P., Durrenberger, M., and Seelig, J. (2005) The cationic cell-penetrating peptide CPP(TAT) derived from the HIV-1 protein TAT is rapidly transported into living fibroblasts: optical, biophysical, and metabolic evidence. *Biochemistry 44*, 138–148.

(30) Tunnemann, G., Martin, R. M., Haupt, S., Patsch, C., Edenhofer, F., and Cardoso, M. C. (2006) Cargo-dependent mode of uptake and bioavailability of TAT-containing proteins and peptides in living cells. *FASEB J. 20*, 1775–1784.

(31) Nakase, I., Tadokoro, A., Kawabata, N., Takeuchi, T., Katoh, H., Hiramoto, K., Negishi, M., Nomizu, M., Sugiura, Y., and Futaki, S. (2007) Interaction of arginine-rich peptides with membrane-associated proteoglycans is crucial for induction of actin organization and macropinocytosis. *Biochemistry 46*, 492–501.

(32) Ter-Avetisyan, G., Tunnemann, G., Nowak, D., Nitschke, M., Herrmann, A., Drab, M., and Cardoso, M. C. (2009) Cell entry of arginine-rich peptides is independent of endocytosis. *J. Biol. Chem. 284*, 3370–3378.

(33) Mitchell, D. J., Kim, D. T., Steinman, L., Fathman, C. G., and Rothbard, J. B. (2000) Polyarginine enters cells more efficiently than other polycationic homopolymers. *J. Pept. Res. 56*, 318–325.

(34) Ziegler, A., and Seelig, J. (2008) Binding and clustering of glycosaminoglycans: a common property of mono- and multivalent cell-penetrating compounds. *Biophys. J. 94*, 2142–2149.

(35) Lundback, T., and Hard, T. (1996) Sequence-specific DNA-binding dominated by dehydration. *Proc. Natl. Acad. Sci. U.S.A. 93*, 4754–4759.

(36) Pace, C. N., Vajdos, F., Fee, L., Grimsley, G., and Gray, T. (1995) How to measure and predict the molar absorption coefficient of a protein. *Protein Sci. 4*, 2411–2423.

(37) Akinc, A., Anderson, D. G., Lynn, D. M., and Langer, R. (2003) Synthesis of poly(beta-amino ester)s optimized for highly effective gene delivery. *Bioconjugate Chem. 14*, 979–988.

(38) Gref, R., Luck, M., Quellec, P., Marchand, M., Dellacherie, E., Harnisch, S., Blunk, T., and Muller, R. H. (2000) 'Stealth' corona-core nanoparticles surface modified by polyethylene glycol (PEG): influences of the corona (PEG chain length and surface density) and of the core composition on phagocytic uptake and plasma protein adsorption. *Colloids Surf., B 18*, 301–313.

(39) van Holde, K. E., Johnson, W. C., and Ho, P. S. (1998) Chemical equilibria involving macromolecules. In *Principles of Physical Biochemistry* (van Holde, K. E., Johnson, W. C., and Ho, P. S., Eds.) pp 604−611, Prentice Hall, Upper Saddle River, NJ.

(40) Schuck, P. (2004) A model for sedimentation in inhomogeneous media. I. Dynamic density gradients from sedimenting co-solutes. *Biophys. Chem. 108*, 187–200.

(41) Miller, K., Shipman, M., Trowbridge, I. S., and Hopkins, C. R. (1991) Transferrin receptors promote the formation of clathrin lattices. *Cell 65*, 621–632.

(42) Williams, S. A., and Buzby, J. S. (2000) Cell-specific optimization of phosphorothioate antisense oligodeoxynucleotide delivery by cationic lipids. *Methods Enzymol. 313*, 388–397.

(43) Pellegrin, P., Fernandez, A., Lamb, N. J., and Bennes, R. (2002) Macromolecular uptake is a spontaneous event during mitosis in cultured fibroblasts: implications for vector-dependent plasmid transfection. *Mol. Biol. Cell 13*, 570–578.

(44) Woodle, M. C., Collins, L. R., Sponsler, E., Kossovsky, N., Papahadjopoulos, D., and Martin, F. J. (1992) Sterically stabilized liposomes. Reduction in electrophoretic mobility but not electrostatic surface potential. *Biophys. J. 61*, 902–910.

(45) Ross, P. C., and Hui, S. W. (1999) Lipoplex size is a major determinant of in vitro lipofection efficiency. *Gene Ther. 6*, 651–659.

(46) Triguero, D., Buciak, J. L., and Pardridge, W. M. (1991) Cationization of immunoglobulin G results in enhanced organ uptake of the protein after intravenous administration in rats and primate. *J. Pharmacol. Exp. Ther. 258*, 186–192.

(47) Ruponen, M., Honkakoski, P., Tammi, M., and Urtti, A. (2004) Cell-surface glycosaminoglycans inhibit cation-mediated gene transfer. *J. Gene Med. 6*, 405–414.

(48) Silhol, M., Tyagi, M., Giacca, M., Lebleu, B., and Vives, E. (2002) Different mechanisms for cellular internalization of the HIV-1 Tat-derived cell penetrating peptide and recombinant proteins fused to Tat. *Eur. J. Biochem. 269*, 494–501.

(49) Gump, J. M., June, R. K., and Dowdy, S. F. (2010) Revised role of glycosaminoglycans in TAT protein transduction domain-mediated cellular transduction. *J. Biol. Chem. 285*, 1500–1507.

(50) Kumagai, A. K., Eisenberg, J. B., and Pardridge, W. M. (1987) Absorptive-mediated endocytosis of cationized albumin and a beta-endorphin-cationized albumin chimeric peptide by isolated brain capillaries. Model system of blood-brain barrier transport. *J. Biol. Chem. 262*, 15214–15219.

(51) King, A. C., and Cuatrecasas, P. (1982) Resolution of high and low affinity epidermal growth factor receptors. Inhibition of high affinity component by low temperature, cycloheximide, and phorbol esters. *J. Biol. Chem. 257*, 3053–3060.

(52) Bretscher, M. S. (1982) Surface uptake by fibroblasts and its consequences. *Cold Spring Harb. Symp. Quant. Biol. 46* (Pt 2), 707–712.

(53) Takeuchi, Y., Sakaguchi, K., Yanagishita, M., Aurbach, G. D., and Hascall, V. C. (1990) Extracellular calcium regulates distribution and transport of heparan sulfate proteoglycans in a rat parathyroid cell line. *J. Biol. Chem. 265*, 13661–13668.

(54) Khalil, I. A., Kogure, K., Akita, H., and Harashima, H. (2006) Uptake pathways and subsequent intracellular trafficking in nonviral gene delivery. *Pharmacol. Rev. 58*, 32–45.

(55) Rejman, J., Conese, M., and Hoekstra, D. (2006) Gene transfer by means of lipo- and polyplexes: role of clathrin and caveolae-mediated endocytosis. *J. Liposome Res. 16*, 237–247.

(56) Duchardt, F., Fotin-Mleczek, M., Schwarz, H., Fischer, R., and Brock, R. (2007) A Comprehensive Model for the Cellular Uptake of Cationic Cell-penetrating Peptides. *Traffic 8*, 848–866.

(57) Kaplan, I. M., Wadia, J. S., and Dowdy, S. F. (2005) Cationic TAT peptide transduction domain enters cells by macropinocytosis. *J. Controlled Release 102*, 247–253.

(58) Lamaze, C., and Schmid, S. L. (1995) The emergence of clathrin-independent pinocytic pathways. *Curr. Opin. Cell Biol. 7*, 573–580.

(59) Wiethoff, C. M., Smith, J. G., Koe, G. S., and Middaugh, C. R. (2001) The potential role of proteoglycans in cationic lipid-mediated gene delivery. Studies of the interaction of cationic lipid-DNA complexes with model glycosaminoglycans. *J. Biol. Chem. 276*, 32806–32813.

(60) Sarhan, S., and Seiler, N. (1989) On the subcellular localization of the polyamines. *Biol. Chem. Hoppe-Seyler 370*, 1279–1284.

(61) Nadel, M. K., Fryer, H. C., and Eisenstark, A. (1957) The probable minimum numbers of Newcastle disease virus particles required to initiate infection in chick embryos and baby chicks. *J. Infect. Dis. 100*, 88–91.

(62) Fretz, M. M., Penning, N. A., Al-Taei, S., Futaki, S., Takeuchi, T., Nakase, I., Storm, G., and Jones, A. T. (2007) Temperature-, concentration- and cholesterol-dependent translocation of L- and D-octa-arginine across the plasma and nuclear membrane of CD34+ leukaemia cells. *Biochem. J. 403*, 335–342.

(63) Matsuya, Y., and Yamane, I. (1985) Cell hybridization and cell agglutination. II. Enhancement of cell hybridization by polycations. *J. Cell Sci. 78*, 273–282.

(64) Coakley, W. T., Hewison, L. A., and Tilley, D. (1985) Interfacial instability and the agglutination of erythrocytes by polylysine. *Eur. Biophys. J. 13*, 123–130.

(65) Zaro, J. L., and Shen, W. C. (2005) Evidence that membrane transduction of oligoarginine does not require vesicle formation. *Exp. Cell Res. 307*, 164–173.

(66) Kosuge, M., Takeuchi, T., Nakase, I., Jones, A. T., and Futaki, S. (2008) Cellular internalization and distribution of arginine-rich peptides as a function of extracellular peptide concentration, serum, and plasma membrane associated proteoglycans. *Bioconjugate Chem. 19*, 656–664.

(67) Tunnemann, G., Ter-Avetisyan, G., Martin, R. M., Stockl, M., Herrmann, A., and Cardoso, M. C. (2008) Live-cell analysis of cell penetration ability and toxicity of oligo-arginines. *J. Pept. Sci. 14*, 469–476.

(68) Subbarao, N. K., Parente, R. A., Szoka, F. C., Jr., Nadasdi, L., and Pongracz, K. (1987) pH-dependent bilayer destabilization by an amphipathic peptide. *Biochemistry 26*, 2964–2972.

(69) Won, Y. Y., Sharma, R., and Konieczny, S. F. (2009) Missing pieces in understanding the intracellular trafficking of polycation/DNA complexes. *J. Controlled Release 139*, 88–93.

(70) Zhou, J., Yockman, J. W., Kim, S. W., and Kern, S. E. (2007) Intracellular kinetics of non-viral gene delivery using polyethylenimine carriers. *Pharm. Res. 24*, 1079–1087.

(71) Kornguth, S. E., Stahmann, M. A., and Anderson, J. W. (1961) Effect of polylysine on the cytology of Ehrlich ascites tumor cells. *Exp. Cell Res. 24*, 484–494.

(72) Sanders, E. J., and Bell, L. G. (1970) Some physiological and morphological effects of polylysine on Amoeba proteus. *J. Cell Sci. 7*, 739–753.

(73) Mayhew, E., Harlos, J. P., and Juliano, R. L. (1973) The effect of polycations on cell membrane stability and transport processes. *J. Membr. Biol. 14*, 213–228.

(74) Kopatz, I., Remy, J. S., and Behr, J. P. (2004) A model for non-viral gene delivery: through syndecan adhesion molecules and powered by actin. *J. Gene Med. 6*, 769–776.

(75) van den Berg, B., and Vink, H. (2006) Glycocalyx perturbation: cause or consequence of damage to the vasculature?. *Am. J. Physiol. Heart Circ. Physiol. 290*, H2174–2175.

(76) Reynwar, B. J., Illya, G., Harmandaris, V. A., Muller, M. M., Kremer, K., and Deserno, M. (2007) Aggregation and vesiculation of membrane proteins by curvature-mediated interactions. *Nature 447*, 461–464.

(77) Zschornig, O., Paasche, G., Thieme, C., Korb, N., Fahrwald, A., and Arnold, K. (2000) Association of lysozyme with phospholipid vesicles is accompanied by membrane surface dehydration. *Gen. Physiol. Biophys. 19*, 85–101.

(78) Magal, L. G., Yaffe, Y., Shepshelovich, J., Aranda, J. F., de Marco Mdel, C., Gaus, K., Alonso, M. A., and Hirschberg, K. (2009) Clustering and lateral concentration of raft lipids by the MAL protein. *Mol. Biol. Cell 20*, 3751–3762.

(79) Janmey, P. A., and Kinnunen, P. K. (2006) Biophysical properties of lipids and dynamic membranes. *Trends Cell Biol. 16*, 538–546.

(80) McNeil, P. L., Miyake, K., and Vogel, S. S. (2003) The endomembrane requirement for cell surface repair. *Proc. Natl. Acad. Sci. U.S.A. 100*, 4592–4597.

(81) Verdurmen, W. P., Thanos, M., Ruttekolk, I. R., Gulbins, E., and Brock, R. (2010) Cationic cell-penetrating peptides induce ceramide formation via acid sphingomyelinase: Implications for uptake. *J. Controlled Release*.

(82) Chen, X., Hou, Y., Tohme, M., Park, R., Khankaldyyan, V., Gonzales-Gomez, I., Bading, J. R., Laug, W. E., and Conti, P. S. (2004) Pegylated Arg-Gly-Asp peptide: 64Cu labeling and PET imaging of brain tumor alphavbeta3-integrin expression. *J. Nucl. Med. 45*, 1776–1783.

(83) Truzzolillo, D., Bordi, F., Sciortino, F., and Cametti, C. (2009) Kinetic arrest in polyion-induced inhomogeneously charged colloidal particle aggregation. *Eur. Phys. J. E: Soft Matter Biol. Phys. 29*, 229–237.

(84) Ziegler, A., Blatter, X. L., Seelig, A., and Seelig, J. (2003) Protein transduction domains of HIV-1 and SIV TAT interact with charged lipid vesicles. Binding mechanism and thermodynamic analysis. *Biochemistry 42*, 9185–9194.

(85) Burak, Y., Ariel, G., and Andelman, D. (2003) Onset of DNA aggregation in presence of monovalent and multivalent counterions. *Biophys. J. 85*, 2100–2110.

(86) Ziegler, A., and Seelig, J. (2007) High affinity of the cell-penetrating peptide HIV-1 Tat-PTD for DNA. *Biochemistry 46*, 8138–8145.

(87) Lentz, B. R. (2007) PEG as a tool to gain insight into membrane fusion. *Eur. Biophys. J. 36*, 315–326.

(88) Rapraeger, A., Jalkanen, M., and Bernfield, M. (1986) Cell surface proteoglycan associates with the cytoskeleton at the basolateral cell surface of mouse mammary epithelial cells. *J. Cell Biol. 103*, 2683–2696.

(89) Edsall, J. T. (1943) Dipolar Ions and acid-base eqilibria. In *Proteins, Amino Acids and Peptides as Ions and Dipolar Ions* (Cohn, E. J., and Edsall, J. T., Eds.) p 75, Reinhold Publishing, New York.